Inorganic Chemistry

pubs.acs.org/IC
Article

Sodium-Poor, Hydroxyl-Rich, Defective $Na_2Ti_3O_7$ Prepared by γ-Irradiation and Its Enhanced Proton Conductivity

Tosapol Maluangnont,* Tanagorn Sangtawesin, Phieraya Pulphol, Orawan Khamman, Pakpoom Reunchan, Kazuma Gotoh, and Naratip Vittayakorn

Cite This: https://doi.org/10.1021/acs.inorgchem.4c02768
Read Online

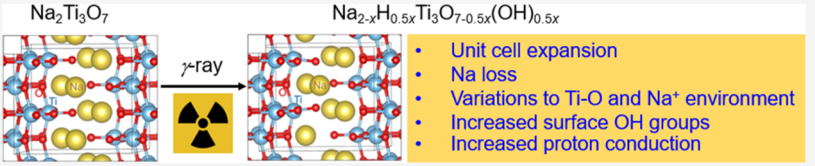

ABSTRACT: The use of γ-irradiation to tailor the physicochemical properties of materials is not widely applied to layered alkali metal oxides. Herein, we show that γ-irradiation (up to 400 kGy) of $Na_2Ti_3O_7$ leads to a sodium-poor, hydroxyl-rich analogue where the layered structure, plate-like morphology, and textural properties are preserved. The deintercalation of sodium ions modifies the Ti−O bond lengths and expands the unit cell; the latter is supported by density functional theory (DFT) calculations. ^{23}Na solid-state NMR suggests the transport of the symmetric, 7-fold Na2 sites to an intermediate environment, which is closer to the asymmetric, 9-fold Na1 sites. An 8 wt % mass loss (1.4 mol water/mol titanate) is observed, indicating an increased concentration of protons/hydroxyls. These hydroxyl groups (i.e., lattice protons) possess higher thermal stability than solely surface-adsorbed ones in the nonirradiated sample. At 200−400 kGy, the proton conduction (50 °C and ∼70% RH) of $\sim 10^{-6}$ S·cm^{-1} is 1 order of magnitude larger than that in the nonirradiated sample; the relaxation time decreases from 30 to 2−6 μs with γ-irradiation. The γ-dose dependence of dielectric loss is also present and analyzed using the Jonscher universal power law, indicating the low-frequency dispersion behavior characteristics of high charge densities.

INTRODUCTION

Sodium trititanate[1] $Na_2Ti_3O_7$ is just one member of a large family of Andersson−Wadsley alkali titanate $A_2O{\cdot}nTiO_2$ (A = alkali, n = integer). The rigid, corrugated $(Ti_3O_7)^{2-}$ layers and the mobile Na^+ ions in two environments (Na1, irregular 9-fold coordinated; and Na2, more symmetric, 7-fold coordinated) form the basis for the early studies on ion exchange/conduction[2] and dielectric properties.[3]

Recently, $Na_2Ti_3O_7$ has demonstrated potential applications as humidity sensors,[4] anode in ion batteries,[5−9] sodium ion capacitors,[10] and solid-state electrolytes.[11] This popularity is due to facile synthesis, micro(nano)structural variation, and various postsynthetic modifications, not to mention environmental friendliness, nontoxicity, and relatively low cost.

The humidity sensitivity of $Na_2Ti_3O_7$ (and other layered alkali titanates) has attracted attention from fundamental and application points of view. Zhang et al.[4] fabricated the $Na_2Ti_3O_7/Al_2O_3$ device as a humidity sensor, showing high humidity sensitivity and quick response−recovery time. Zarrabeitia et al.[7] reported the partial formation of the solid solution $Na_{2-x}H_xTi_3O_7$ by humid air exposure up to 8 weeks. In a series of works, we have reported the water-induced charge transport in lepidocrocite titanate[12,13] or TiO_2-containing composites,[14] including their electrical property signatures. The sensitivity to water can be easily detected as hysteresis in a heating/cooling experiment due to the variation in the adsorbed water content.[5,12,13]

The interlayer Na^+ ions in $Na_2Ti_3O_7$ can be exchanged with protons, producing $H_2Ti_3O_7{\cdot}0.8H_2O_{ads}$[15] (the subscript ads indicates surface-adsorbed) with the conductivity of 5.5×10^{-6} S·cm^{-1} (vs $\sim 2 \times 10^{-6}$ S·cm^{-1} in $Na_2Ti_3O_7$[11] or $\sim 1 \times 10^{-7}$ S·cm^{-1} in 1/1 the $Na_2Ti_3O_7/Na_2Ti_6O_{13}$ composite[16]). In contrast to the volume transport of intercalated protons, the understanding of surface protonic conduction[17] in alkali titanates is much more limited. Here, we focus on noncrystalline waters located at the crystal edge, external surface, grain boundary, or porosity. They could be removed at ≤300 °C, while the layered structure is preserved, unlike the thermally unstable protonic analogues.[15,18] This feature is well suited to applications such as low-temperature proton-conducting ceramics,[17] where the conductivity up to $\sim 2 \times 10^{-3}$ S·cm^{-1} was reported in perovskite-type $BaZr_{0.85}Y_{0.15}O_3$ (350 °C, 2.3% water in N_2).

Received: July 3, 2024
Revised: September 3, 2024
Accepted: September 9, 2024

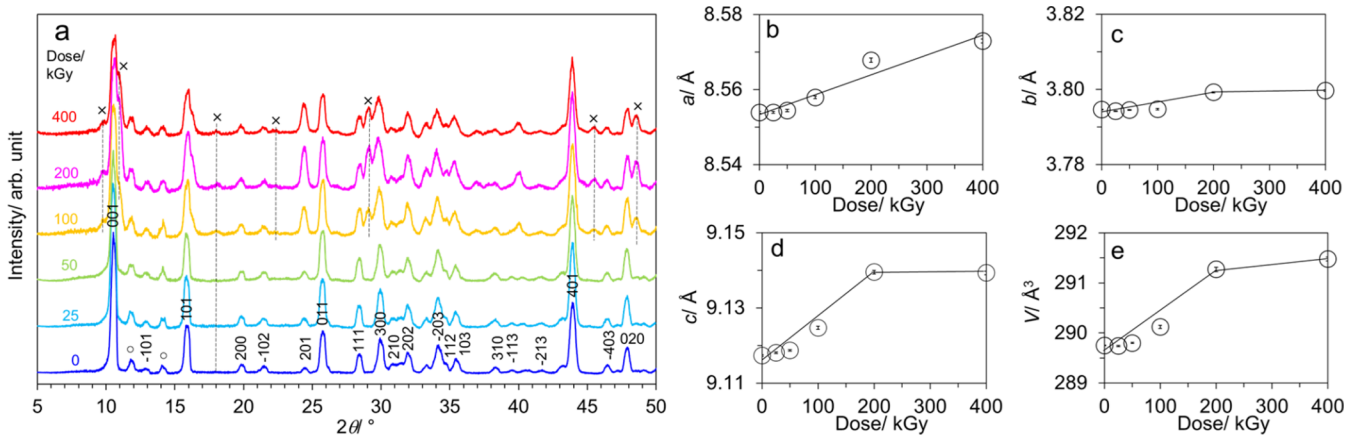

Figure 1. (a) XRD patterns of $Na_2Ti_3O_7$ at different doses of γ-irradiation and the dose-dependent evolution of unit cell parameters: (b) *a*, (c) *b*, (d) *c*, and (e) *V*. The standard deviations from the refinement in parts b-e are smaller than the size of the symbols.

Because proton exchange is cumbersome and lengthy and generates a lot of waste, an improved procedure is desirable to generate proton-conducting materials. Gamma (γ)-irradiation, on the one hand, is employed to investigate the suitability of materials in nuclear applications, such as Li_2TiO_3 (rocksalt, not layered structure) which is a tritium breeder.[19] On the other hand, γ-irradiation is a dry, chemical-free, and waste-free method that can be conducted using a commercial γ-chamber at already existing nuclear facilities at no additional costs to tailor the physicochemical properties of materials.[20−25] For example, the γ-irradiation of TiO_2 single crystals[20] led to the formation of an oxygen vacancy and the reduction of Ti^{4+} to Ti^{3+}. At the optimum dose of γ-irradiation, an increase in conductivity or dielectric permittivity has been reported in Co−Fe-layered double hydroxide (Co−Fe LDH),[21] mica,[22] graphite,[23] $TlInS_2$,[24] and graphite fluoride,[25] due to structural deformations or the formation of functional groups (e.g., hydroxyl). Interestingly, these examples contrast with the γ-shielding property of titanate nanosheets[26] which decelerate cellulose degradation from γ-irradiation. For alkali titanates, it is known that interlayer ion vacancies are generated by high-temperature sintering,[27−29] ball-milling,[30,31] or reaction with reagents such as poly(tetrafluoroethylene).[32] The Na vacancy, in turn, leads to an oxygen vacancy to preserve charge neutrality. Recent density functional theory (DFT) calculations have shown that sodium vacancy and oxygen vacancy are the most abundant defects in $Na_2Ti_3O_7$.[33,34] Abass and Seriani limitedly reported[34] that the Na-poor analogue has the expanded unit cell.[34] However, it is not clear how these findings are related to γ-irradiated layered alkali titanate.

In this work, we investigate the influence of γ-irradiation (up to 400 kGy) on proton conduction in $Na_2Ti_3O_7$ using alternating current (AC) impedance spectroscopy. Studies of proton conduction typically benefit from variable conditions including relative humidity (RH) (or water partial pressure), surrounding gas, temperature, and so on. Such dedicated setups provide a wealth of information, but they are demanding and expensive. Alternatively, one can utilize characteristics such as water loss at elevated temperatures, water (re)adsorption during cool down, and hysteresis of electrical properties of closely related samples under similar (yet not as rigorously controlled) conditions. This latter approach[12,35] has been proven to be useful in other compositions of layered alkali titanates, which is to be applied here. The samples were characterized across multiple length scales from microstructure (i.e., morphology) to long-range and local structure, in addition to investigations on composition, surface functionals, and thermal stability. We also employ DFT calculations to further support the experimental findings regarding the unit cell expansion and to deduce the valence state[36] on Ti atoms. Our present work on the defects chemistry of γ-irradiated $Na_2Ti_3O_7$ layered crystals contrasts with chemical-based postsynthetic modifications,[8−10,16] presenting an alternative method which could be applicable to other layered alkali metal oxides.

EXPERIMENTAL SECTION

$Na_2Ti_3O_7$ is a commercial product from Sigma-Aldrich and was used as received. Separated portions of the titanate were subjected to γ-irradiation from the ^{60}Co source (Ob-Servo Ignis, Izotop, Hungary, 10 kGy·h^{-1}) to accumulated doses of 25, 50, 100, 200, and 400 kGy at ∼25 °C, 40% RH, and under static air, in addition to the nonirradiated one. Without any other workup or contact with liquids, the samples were kept in a glass vial under ambient conditions and were characterized as described in the Supporting Information.

Approximately 0.3 g of the powder was pressed into a pellet with a diameter of ∼1 cm and a thickness of ∼0.15 cm without a binder. The apparent densities of the pellets were 72−77% of the theoretical density, and they did not vary systematically with the γ-dose. All pellets were coated with silver paint on both surfaces and subsequently dried overnight at room temperature (RT). The complex impedance measurements were conducted using a precision LCR meter (HP-4284A, Hewlett-Packard, Palo Alto, CA) covering the frequency f = 20 to 10^6 Hz and RH ∼ 70%. The temperature-scan experiment was performed for one cycle (RT → 350 °C → RT; 2 °C·min^{-1}) during which the impedance was measured without dwelling at any temperature. Later on, only the data at 50 °C were compared to highlight the effect of γ-irradiation on proton conduction. The measured complex impedance was then converted to conductivity σ_{AC} and the imaginary part of the complex dielectric permittivity ε'' by standard equations.[14,37]

The DFT calculations were performed using the generalized gradient approximation (GGA) proposed by Perdew, Burke, and Ernzerhof, revised for solids (PBEsol),[38] as implemented in the VASP code.[39,40] Details can be found in the Supporting Information.

RESULTS AND DISCUSSION

Long-Range Structure and Composition. Figure 1a shows the X-ray diffraction (XRD) patterns of all $Na_2Ti_3O_7$ samples, which are typical of the sodium trititanate structure ($P2_1/m$),[1] except those (○) due to $Na_2Ti_6O_{13}$ impurity

https://doi.org/10.1021/acs.inorgchem.4c02768
Inorg. Chem. XXXX, XXX, XXX−XXX

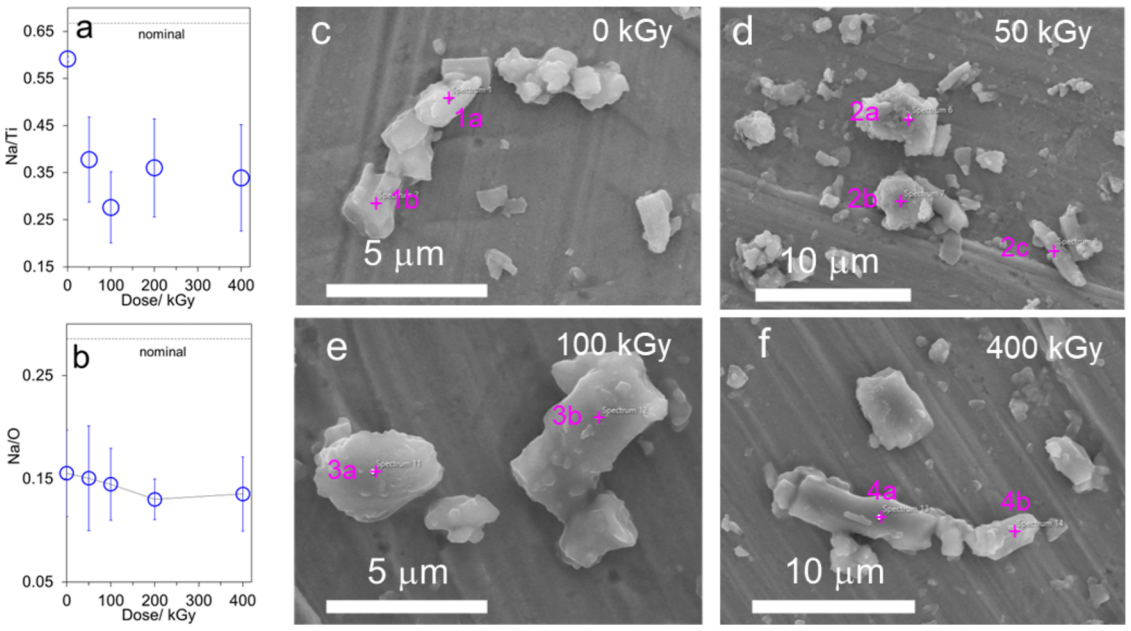

Figure 2. Dependence of (a) Na/Ti and (b) Na/O on the γ-dose, and the SEM images of $Na_2Ti_3O_7$ at (c) 0, (d) 50, (e) 100, and (f) 400 kGy. The positions shown in pink in pannels (c–f) correspond to those in Table S2 and Figure S3.

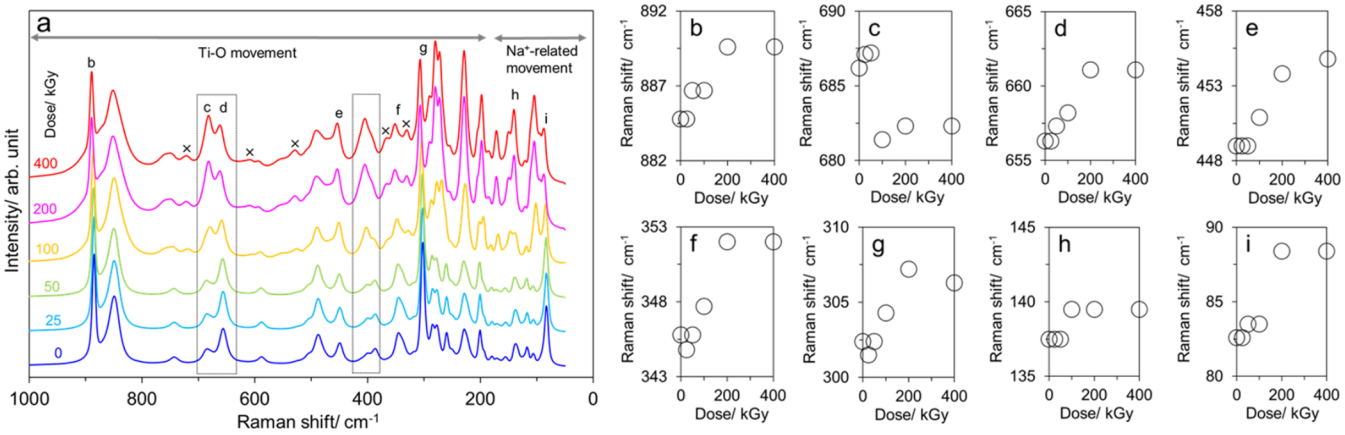

Figure 3. (a) Raman spectra of $Na_2Ti_3O_7$ at different doses of γ-irradiation and (b)-(i) the dose-dependent evolution of some peak positions as labeled in pannel (a).

already present in the nonirradiated sample. Upon γ-irradiation, the peaks are gradually broadened and asymmetric with reflections due to the $H_2Ti_3O_7$ impurity (×, Figure S1) appearing at ≥100 kGy. Figure 1b–e shows the evolution of the unit cell parameters refined with JANA[41] (see also Table S1 and Figure S2). They mostly increase with doses from 0 to 200 kGy, followed by a stabilization up to 400 kGy. Notably, increasing c [9.1173(2)–9.1395(5) Å, +0.24%] is along the stacking direction, indicating interlayer expansion. For comparison, the interlayer distance increased in irradiated bentonite (~1 Å, 6%),[42] decreased in irradiated graphite (0.3%),[23] and remained unchanged in irradiated Co–Fe LDH.[21]

The interlayer expansion (without guest intercalation) has been reported due to thermal expansion,[5] high-temperature sintering,[27−29] or ball-milling.[30,31] At room temperature, this is typically ascribed to a partial alkali ion deintercalation, which reduces the electrostatic interaction between the positively charged interlayer ions and the negatively charged titanate sheets. Energy-dispersive X-ray (EDX) analyses on the nonirradiated $Na_2Ti_3O_7$ yield Na/Ti = 0.592(6) (the number in parentheses is the standard deviation to the last digit) compared to the nominal value of 0.667. This finding indicates that the experimentally determined Na/Ti is underestimated, but this is consistent across all samples. It is found that Na/Ti decreases from 0.592(6) to 0.3(1) as the γ-dose increases from 0 to 400 kGy; see Figure 2a and Table S2. Decreasing Na/Ti implies the formation of a sodium vacancy, which is the most favorable defect according to the recent DFT calculations.[33,34] In a supporting manner, Na/O decreases [0.16(4)–0.14(4)] with the dose. The change in these ratios occurs from 0 to ~200 kGy followed by a stabilization after that, roughly following the variations of unit cell parameters. We recently reported[25] decreasing F/C with increasing γ-dose in graphite fluoride $(CF)_n$, a van der Waals layered material. We are not aware of other reports on the γ-irradiation-induced deintercalation of the interlayer ions. The compositional variation occurs while the plate-like morphology is well preserved regardless of the γ-dose (see Figure 2c–f).

https://doi.org/10.1021/acs.inorgchem.4c02768
Inorg. Chem. XXXX, XXX, XXX−XXX

Local Structure. The long-range modification and compositional changes affect the local structure, as deduced from the Raman spectra in Figure 3a. These Raman bands are typical of $Na_2Ti_3O_7$,[43−45] except the impurity bands (×) at 100−400 kGy. There is a consensus[43−45] that bands due to Ti−O movements are at >200 cm^{-1}, while those related to the interlayer Na^+ are at <200 cm^{-1}. Notably, there is a gradual upshift of almost all bands with γ-irradiation. Let us consider as an example the most energetic band at 885 cm^{-1} (vs 884−890 cm^{-1} in refs 43−45). This is the Ti−O symmetric stretching of the O atom in the corner of the ribbon. The upshift shown in Figure 3b indicates the shortening of the bond (which is observed in almost all peaks, Figure 3d−i). The only downshift is shown in Figure 3c at 686 cm^{-1} (vs 684 cm^{-1} in ref 43) ascribed to the asymmetric deformation of Ti−O, indicating Ti−O bond lengthening. The finding that shortened Ti−O bonds are accompanied by an expanded unit cell is at first surprising. However, this could suggest that diminishing electrostatic forces (interlayered Na^+ ions/$Ti_3O_7^{2-}$ sheets) have a dominating effect on unit cell parameters compared to the increased van der Waals forces at the sheets. In addition, the relative peak intensity also changes (e.g., bands c and d) or some bands merge (in the box at ∼400 cm^{-1}). However, it is not possible to interpret the data without a single crystal and a polarized light.

It is also noted that the Raman bands at <200 cm^{-1} are complicated and significantly change in relative intensity, implying the change in the local environment of Na^+ ions due to the γ-irradiation. This is supported by an examination of the ^{23}Na solid-state NMR spectra. The spectrum of nonirradiated $Na_2Ti_3O_7$ (Figure 4) is similar to others,[6−9] consisting of two

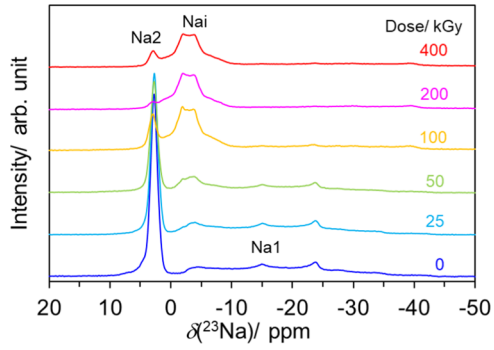

Figure 4. ^{23}Na NMR spectra of $Na_2Ti_3O_7$ at different doses of γ-irradiation.

main signals. The narrow value at ∼2.7 ppm is ascribed to Na at the high symmetry site (Na2, 7-fold). The broad component including the peak between −15 and −21 ppm is due to Na at the low symmetry sites (Na1, 9-fold). In addition, there is a much broader component (suggesting the amorphous character) at 0 to −15 ppm similar to the spectrum of $Na_2CO_3{\cdot}H_2O$.[6] This finding does not contradict the assignment of the impurity as $H_2Ti_3O_7$ because NMR is capable of detecting a minor phase otherwise invisible to other techniques. A small amount of carbonate is understandable, considering that the lattice oxygen molecules are the basic sites, reacting with acid CO_2 molecules in the air.[46] Upon γ-irradiation, the Na2 signal greatly decreases in intensity, consistent with its higher mobility as suggested by the proton exchange experiment.[7] Meanwhile, another signal at −1.6 to −3.4 ppm (denoted Nai) which is intermediate between Na2 and Na1 has clearly gained intensity at ≥100 kGy, coinciding with the impurity peaks (×) due to $H_2Ti_3O_7$ in Figure 1a. Because proton occupies the interlayer spaces, it is reasonable that sodium ions relocate to avoid electrostatic repulsions, although the exact surroundings of this Nai remain to be elucidated.

DFT Calculations. Na loss implies the formation of Na vacancies, which is studied in detail here. The calculated formation energies for Na vacancies (V_{Na}) (and Ti vacancies V_{Ti}, for comparison) under O-poor and O-rich limits are shown in Figure 5a,b. (These limits represent O-poor/metal-rich and O-rich/metal-poor conditions, respectively, which are described according to the chemical potentials of Na, Ti, and O, following the report by Choi et al.[33]) It is found that V_{Na} acts as a single acceptor (i.e., producing one hole) and is stable exclusively in the 1- charge state, consistent with the fact that Na^+ is an alkali ion. For V_{Ti}, it can occur in the neutral, 1-, 2-, 3-, and 4-, charge states, also consistent with the fact that Ti has four valence electrons. Notably, V_{Na} has a much lower formation energy than V_{Ti} in both limits for the Fermi levels near the valence band maximum. Hence, creating sodium vacancies should be much easier even under nonequilibrium conditions such as γ-irradiation. Our calculation sufficiently reflects the stability of sodium-poor samples; the incorporation of hydroxyl groups is too complicated and is not presently considered.

We investigate the impact of V_{Na} on the lattice parameters of $Na_2Ti_3O_7$ by first removing one Na atom from the 48-atom supercell (Figure 5c,d), which corresponds to 12.5% V_{Na} (Na/Ti = 0.58). The equilibrium lattice parameters shown in Table 1 are larger than those of the (calculated) 0% V_{Na}, consistent with the experimentally observed expansion upon γ-irradiation and with the limited DFT calculations[34] by others. Next, another Na atom was removed such that there were two sodium vacancies (V_{Na} = 25%; Na/Ti = 0.50). (Na/Ti = 0.50−0.58 fall between those determined by EDX at 0 and 50 kGy; see Figure 2a.) The two scenarios in which (i) the two V_{Na} are formed next to each other (V_{Na}−V_{Na} distance = 3.91 Å) or (ii) separate from each other (V_{Na}−V_{Na} distance = 5.45 Å) are considered. However, they result in similar unit cell volumes and lattice parameters. Importantly, unit cell parameters keep increasing with V_{Na}, in good agreement with XRD results.

It is found that the average Bader charge at Ti atoms of the pristine $Na_2Ti_3O_7$ is 2.18(1) (the number in parentheses is the standard deviation to the last digit). The Bader charge remains practically constant in the Na-poor sample (12.5% V_{Na}) at 2.16(4). These number are close to the calculated Bader charge of Ti^{4+} in TiO_2 (rutile) of 2.28 (vs 2.24 in ref 36), which are significantly different from that of Ti^{3+} in Ti_2O_3 of 1.88. Accordingly, DFT suggests that Ti is tetravalent. This is consistent with the white color of all samples, regardless of γ-dose. Otherwise, the titanate will be deep blue as in the $K_2(Ti^{4+})_{6-2x}(Ti^{3+})_{2x}O_{13-x}$ prepared by a high-temperature reduction of $K_2(Ti^{4+})_6O_{13}$ with H_2.[47]

Surface Water and Hydroxyl Groups. The $Na_2Ti_3O_7$ samples were subjected to TG analysis. As shown in Figure 6a, the samples at low γ-doses (0−50 kGy) show negligible mass loss (RT-200 °C, ∼0.7 wt %) ascribed to the loss of water adsorbed on the surfaces. In contrast, the samples at high doses show three distinct mass loss regions from RT-150, 150−500, and >500 °C (see also the derivative curves). The latter two stages are ascribed to lattice water (and the accompanying

https://doi.org/10.1021/acs.inorgchem.4c02768
Inorg. Chem. XXXX, XXX, XXX−XXX

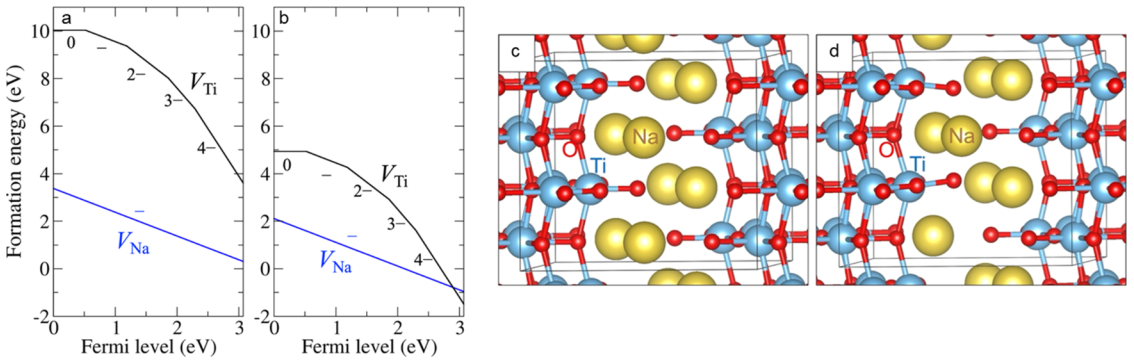

Figure 5. Formation energies of V_{Na} and V_{Ti} as a function of the Fermi level at the (a) O-poor and (b) O-rich limits. The slope of each line reflects the charge state. Only the lowest energy charge state of each defect is shown. The local atomic structure of the 48-atom supercell of (c) pristine $Na_2Ti_3O_7$ and (d) 12.5% V_{Na}. The supercell is displayed by solid lines.

Table 1. Calculated Unit Cell Parameters of $Na_2Ti_3O_7$ at Different Contents of V_{Na}

sample	Na/Ti	a/ Å	b/Å	c/Å	β/°	V/Å^3
nonirradiated[a]	0.592	8.5539(3)	3.7943(1)	9.1173(2)	101.74	289.75(1)
0% V_{Na}	0.667	8.56	3.79	9.12	101.81	289.63
12.5% V_{Na}	0.583	8.601	3.808	9.164	101.86	293.75
25% V_{Na}	0.500	8.642	3.827	9.208	101.86	298.00

[a]XRD.

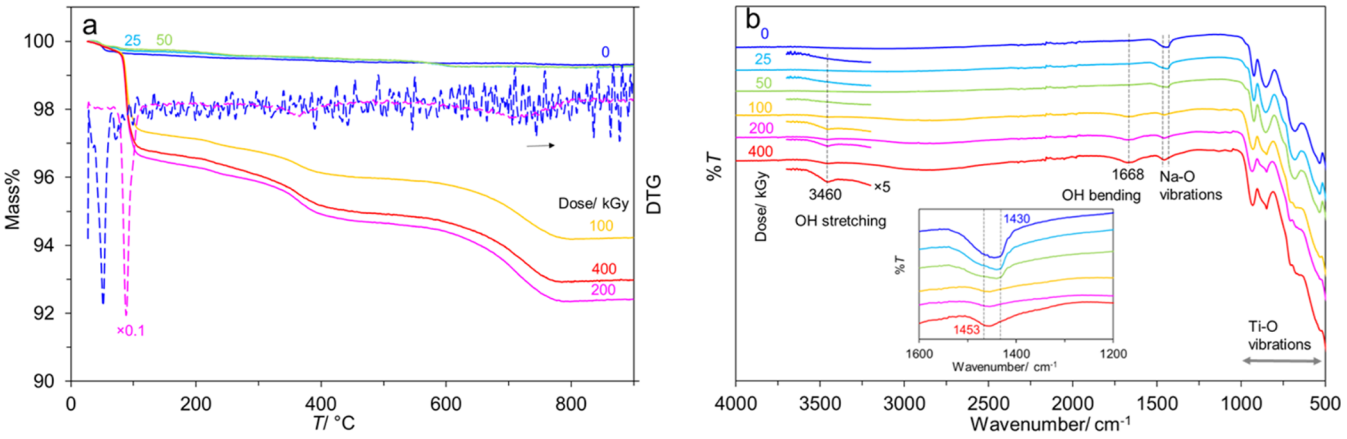

Figure 6. (a) Mass loss curves and selected derivative curves and (b) IR spectra of $Na_2Ti_3O_7$ at different doses of γ-irradiation.

Table 2. Summary of Mass Loss, Mol Water/Mol Titanate, and E_a of the $Na_2Ti_3O_7$ Samples at Different Doses of γ-Irradiation

			E_a[c]/kJ·mol^{-1}			
dose/kGy	mass loss[a]/wt %	y[b]	LT1	LT2	MT	HT
0	0.68	0.11	69	69	not observed	not observed
25	0.73	0.12	NA[d]	NA	NA	NA
50	0.72	0.12	87	[e]	153	158
100	5.77	1.03	NA	NA	NA	NA
200	7.59	1.38	NA	NA	NA	NA
400	7.02	1.26	102	95	136	140

[a]Mass loss from RT to 900 °C from TGA. [b]Assuming the ideal composition $Na_2Ti_3O_7{\cdot}yH_2O_{ads}$. [c]From DSC analysis (Figure 7) and using eq 1. [d]Not available. [e]Not determined. The LT2 peaks heavily overlap with the LT1 peaks.

dehydroxylation), as it is unlikely that merely physisorbed water would persist to such a high temperature. At 900 °C, mass losses equal to 5.8, 7.6, and 7.0 wt % were observed for the samples irradiated at 100, 200, and 400 kGy, respectively. (These are comparable to the theoretical mass loss[48] (7.0 wt %) for the dehydration of the protonic analogue: $H_2Ti_3O_7 \rightarrow H_2O + 3TiO_2$.) The observed mass loss in our sample corresponds to ~0.1−1.4 mol water/mol $Na_2Ti_3O_7$ (Table 2), which increases with the γ-dose.

In a supporting manner, infrared (IR) spectra in Figure 6b are typical of $Na_2Ti_3O_7$[45] which is the major phase (and unlike $H_2Ti_3O_7$[48]), showing several Ti−O vibrations at ~500−1000 cm^{-1}. The OH stretching/bending at 3460/1668 cm^{-1} gains in intensity, especially at 100−400 kGy. Note that the increasing

https://doi.org/10.1021/acs.inorgchem.4c02768
Inorg. Chem. XXXX, XXX, XXX−XXX

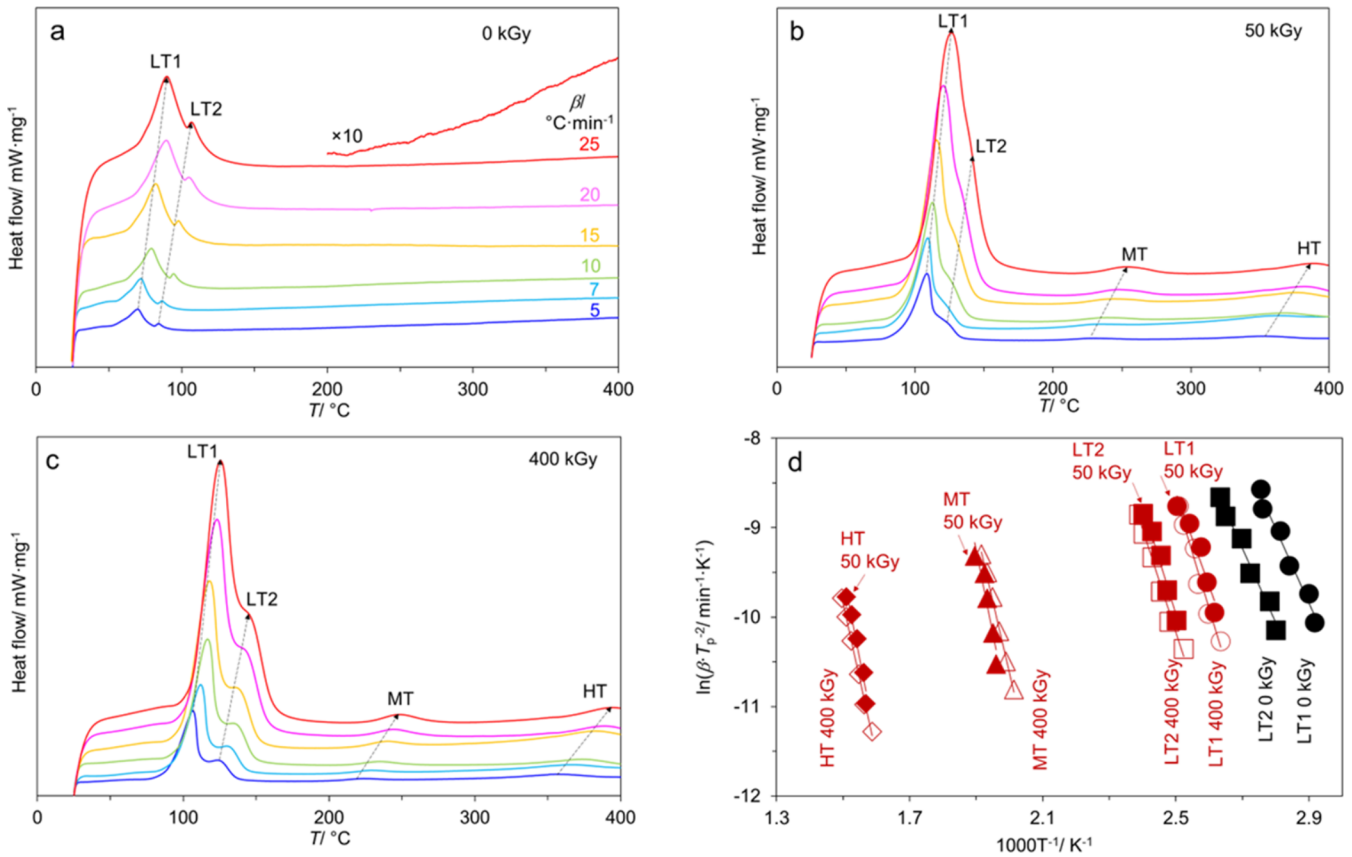

Figure 7. Heat flow curves of $Na_2Ti_3O_7$ at different doses of γ-irradiation: (a) 0, (b) 50, and (c) 400 kGy; (d) the corresponding Kissinger plots.

water or hydroxyl content is not due to the increasing surface area/pore diameter, which is practically constant (44 to 55 $m^2 \cdot g^{-1}$/4.3−4.6 nm) as shown in Figure S4 and Table S3. The peaks at 1430−1453 cm^{-1} are ascribed to Na−O vibrations,[45] which clearly change in shape and position (inset in Figure 6b), further confirming that this moiety is affected by γ-irradiation. The peaks due to carbonate at ∼1345−1575 cm^{-1} (which are usually strong)[12,13,27] are absent. Hence, the amount of carbonate-containing impurities detectable from ^{23}Na NMR experiments must be low.

Selected $Na_2Ti_3O_7$ samples were subjected to differential scanning calorimetry (DSC) analyses from RT to 400 °C at varying heating rates. Figure 7a shows the heat flow curves of the nonirradiated sample, where two endothermic peaks (LT1, LT2) with peak temperatures T_p (typically lower than 107 °C) are observed. Upon γ-irradiation at 50 and 400 kGy (Figure 7b,c), the LT1 and LT2 peaks overlap and additional peaks at medium (MT) and high (HT) temperatures can be observed. We apply the Kissinger equation[49]

$$\ln(\beta/T_p^2) = -(E_a/RT_p) + \ln(AR/E_a) \quad (1)$$

where β is the heating rate in °C·min^{-1}, E_a is the apparent activation energy in kJ·mol^{-1}, R is the universal gas constant, and A is the preexponential factor. Figure 7d shows that $\ln(\beta/T_p^2)$ vs $1000/T_p$ is the straight line. The slope of the plot provides the activation energies listed in Table 2. These numbers are comparable to ∼81−83 kJ·mol^{-1} (titanate nanotubes) and 116−139 kJ·mol^{-1} ($H_2Ti_3O_7$),[50] both with intercalated water. Hence, γ-irradiation generates hydroxyl groups (i.e., lattice water) with increased thermal stability, which are clearly different from merely physisorbed water in pristine $Na_2Ti_3O_7$.

Taken together, we propose eqs 2 and 3 to describe the γ-irradiation-induced modification to pristine $Na_2Ti_3O_7$

$$Na_2Ti_3O_7 \rightarrow Na_{2-x}Ti_3O_{7-0.5x} + 0.5xNa_2O \quad (2)$$

$$Na_{2-x}Ti_3O_{7-0.5x} + 0.5xH_2O \rightarrow Na_{2-x}H_{0.5x}Ti_3O_{7-0.5x}(OH)_{0.5x} \quad (3)$$

Equation 2 is the Na^+ deintercalation and its subsequent transformation to Na_2O. Because Na/Ti is found to decrease, the formed Na_2O must be removed, presumably by reacting with gases in the irradiation chamber (i.e., H_2O (40% RH) or an unmeasured amount of CO_2) to volatile species. The effects of surroundings during γ-irradiation deserve further investigation. The removal of xNa^+ requires the release of $0.5xO^{2-}$, thereby generating an oxygen vacancy.[13,28,29] Then, the $Na_{2-x}Ti_3O_{7-0.5x}$ intermediate reacts with atmospheric water as shown in eq 3. The $0.5x$ unit of the O-vacancy is filled with an equal amount of a hydroxyl group. To preserve charge neutrality, another $0.5xH^+$ ion could be incorporated into the sample. This scheme is consistent with the formation of a $H_2Ti_3O_7$-like impurity in Figures 1 and S1. The contract d spacing further supports the limited incorporation of H^+ (but not H_3O^+ which is larger than Na^+) as widely known experimentally[2] and computationally.[34] The interlayer contraction due to Na^+/H^+ exchange is known when $Na_2Ti_3O_7$ was in contact with liquid water,[16] or acidic aqueous solution of a polymer,[16] or exposed to humid air (up to 8 weeks).[7]

https://doi.org/10.1021/acs.inorgchem.4c02768
Inorg. Chem. XXXX, XXX, XXX−XXX

Taking it all together, defective sodium trititanate $Na_{2-x}H_{0.5x}Ti_3O_{7-0.5x}(OH)_{0.5x}$ is produced, where Ti atoms remain tetravalent. These incorporated protons could be responsible for a massive TG loss (Figure 6a), an increased E_a of dehydroxylation (Table 2), an increasing intensity of OH stretching/bending vibrations (Figure 6b), and many endothermic events (Figure 7), including the enhanced proton conduction to be discussed in the next section.

Proton Conduction and Other AC Electrical Properties. We first examine the AC conductivity σ_{AC} (eq(S1)) of nonirradiated $Na_2Ti_3O_7$ subjecting to a temperature program RT → 350 °C → RT. Two representative frequencies at 10^6 Hz and 10^2 Hz are shown in Figure 8, which are the high and low limits, respectively, of our instrument. At 10^6 Hz, σ_{AC} increases very slightly from RT to ∼100 °C due to the increased thermal energy of charge carriers (protons). At 100−150 °C, σ_{AC} decreases by 2 orders of magnitude because of proton loss (water evaporation). These two stages coincide with a much sharper endothermic peak detected by DSC as shown in Figure 8. Then, σ_{AC} increases with increasing temperature (at 350 °C, it reaches the original value at RT) due to the increased thermal energy of charge carriers such as Na^+ ions or electrons/holes. (The origin of the small peak at ∼270 °C is not known at present.) In the subsequent cooling, σ_{AC} decreases because charge carriers possess decreased thermal energy. Interestingly, σ_{AC} increases again at <100 °C and finally matches the value at the beginning of the measurement. The same behavior is observed at all frequencies (shown as another example at 10^2 Hz in Figure 8). Such a hysteresis in the AC electrical properties of humidity-sensitive ceramics can be well explained[5,12,35,51,52] by a competition between water loss and water (re)adsorption in the overall charge transport. Typical conduction by Na^+ ions or electrons/holes is unlikely to show such a feature. Hence, it is deduced that proton conduction in $Na_2Ti_3O_7$ dominates at ambient, where other charge carriers could contribute less to the overall process. A humidity-controlled measurement or an H/D isotope exchange will provide additional insights such as kinetics or mobility, but these are not available at present.

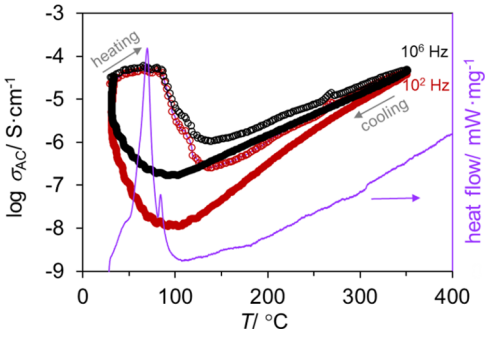

Figure 8. Temperature-dependent log σ_{AC} at 10^6 and 10^2 Hz of the nonirradiated $Na_2Ti_3O_7$ subjected to a temperature program RT → 350 °C → RT; also shown is the DSC heat flow curve (up for endothermic).

To emphasize the proton conduction in γ-irradiated $Na_2Ti_3O_7$ samples, only the data at 50 °C (i.e., prior to the heating) acquired under a typical laboratory atmosphere (∼70% RH) will be discussed. Figure 9a shows the Nyquist plots of all samples as a single depressed semicircle. Because the powder was simply pressed into a pellet without sintering, it is reasonable to assume that these signals are due to the grain boundary response. Considering the simplified pathways for proton conduction,[14,17] the protons could be (i) along the grain boundary, (ii) open pores' surfaces, and (iii) in a proton-enriched layer directly below the pore/oxide interfaces. These pathways should dominate in the present case, in addition to (iv) conduction at the bulk, which is not as significant except at higher doses. If so, proton conduction will depend on parameters such as particle size, pellet density, heating/cooling rates, etc., which are to be reported elsewhere.

The decreased diameter of the semicircle suggests that the samples are more conducting with increasing γ-dose. Figure 9b shows that σ_{AC} decreases with decreasing f as commonly

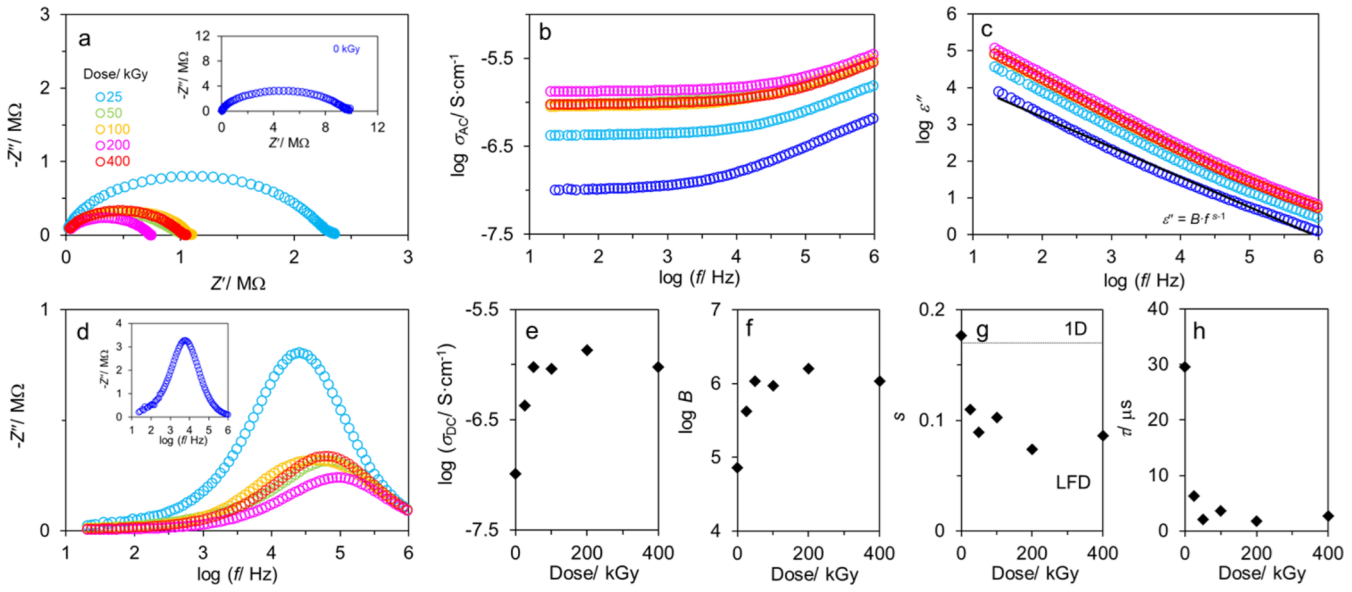

Figure 9. AC properties of the $Na_2Ti_3O_7$ samples at different doses of γ-irradiation: (a) Nyquist plots and the f-dependence of (b) log σ_{AC}, (c) log ε'', and (d) $-Z''$, the dose dependence of (e) log σ_{DC}, (f) log B, (g) s, and (h) τ. Insets in parts a and d show the data at 0 kGy. The full line in part (c) is the fit to the equation. The dashed line in part (g) is the boundary between the 1D and LFD. All data were taken at 50 °C.

https://doi.org/10.1021/acs.inorgchem.4c02768
Inorg. Chem. XXXX, XXX, XXX−XXX

observed in layered alkali titanates,[12,13,29,53,54] prior to an f-independent plateau σ_{DC}. Due to the enriched proton, the conductivity increases with γ-irradiation from 1.0×10^{-7} S·cm^{-1} (nonirradiated) to 1.3×10^{-6} S·cm^{-1} (200 kGy) (the latter is comparable to 2×10^{-6} S·cm^{-1} in nonirradiated, sonochemically prepared $Na_2Ti_3O_7$ nanoparticles[11]). A slight decrease in σ_{DC} at 400 kGy (9.5×10^{-7} S·cm^{-1}) is consistent with the reduced water content, which might be affected by structural disordering at high doses, thereby inhibiting proton transport. The promoted σ_{DC} at 200 kGy is comparable to that in $H_2Ti_3O_7{\cdot}0.8H_2O_{ads}$[15] and other proton-intercalated layered titanates (see Table S4). The effect of the $Na_2Ti_6O_{13}$ impurity should be similar at all doses, as its content is small and its diffraction peaks (○ in Figure 1a) remain unchanged. Otherwise, Baliteau et al.[55] reported that $Na_2Ti_3O_7$ is more conducting than $Na_2Ti_6O_{13}$, but Choi et al.[33] reported the opposite. The enhancement of σ_{DC} is by a factor of 10 in the present case, vs 4 in mica[22] and 100 in graphite,[23] depending on materials properties, which awaits exploration.

Figure 9c shows the dielectric loss ε'' [eq(S2)] on a log scale. It is found that $\log \varepsilon''$ decreases with increasing f, consistent with the previous works.[53] $\varepsilon''(f)$ can be fit (i.e., straight line) using the Jonscher universal power law[12,53,56,57] due to interacting charges/dipoles

$$\varepsilon'' = B{\cdot}f^{s-1} \tag{4}$$

where B and s are the fitting parameters. The dose dependence of B and s are shown, respectively, in Figure 9f,g. Specifically, s is mostly close to zero (i.e., $\varepsilon'' \sim f^{-1}$). This is known as the "low-frequency dispersion"[53,58] which indicates that very high charge densities are being stored either "along" the interfaces/humid surfaces or "across" interfaces, consistent with surface proton conduction across grain boundary.

Lastly, Figure 9d shows log $-Z''(f)$ where a relaxation peak is observed and the exact position depends on the dose. Equation 5 is employed to calculate the relaxation time τ

$$\tau = 1/(2\pi f_{max}) \tag{5}$$

where f_{max} is the position of the peak maximum. As summarized in Figure 9h, τ decreases from ~30 μs to 2−6 μs as the γ-dose increases. Accordingly, it is easier for charge carriers to respond to the applied external electric field thanks to γ-irradiation. The magnitudes of τ in microseconds are similar to other layered alkali titanates,[53,54] which are very small (i.e., much quicker relaxation) compared to 78 s in the $Na_2Ti_3O_7/Na_2Ti_6O_{13}$ composite.[16]

CONCLUSIONS

The defective samples of $Na_2Ti_3O_7$, prepared by γ-irradiation (up to 400 kGy), have reduced crystallinity with variations in Ti−O bond lengths and altered local structure of the Na ions. While the platy microstructure is preserved, a gradual Na loss is deduced. This is accompanied by the uptake of atmospheric water, forming hydroxyl groups with varying thermal stability, depending on the γ-dose. We proposed equations to account for these findings, including (i) sodium loss, (ii) hydroxyl group formation, and (iii) additional proton incorporation, where Ti atoms remain tetravalent. It is proposed that the increased proton concentration is the major factor responsible for the enhanced proton conduction in the sodium-poor, hydroxyl-rich $Na_2Ti_3O_7$. The present findings suggest γ-irradiation as a chemical- and waste-free method to alternatively alter the physical properties of other layered alkali titanate.

ASSOCIATED CONTENT

Supporting Information

The Supporting Information is available free of charge at https://pubs.acs.org/doi/10.1021/acs.inorgchem.4c02768.

Experiments; tabulation of unit cell parameters and LeBail fitting; additional EDX analyses and SEM images; N_2 adsorption/desorption isotherms; and tabulation of conductivity (PDF)

AUTHOR INFORMATION

Corresponding Author

Tosapol Maluangnont − *College of Materials Innovation and Technology, King Mongkut's Institute of Technology Ladkrabang, Bangkok 10520, Thailand; Advanced Materials Research Unit, School of Science, King Mongkut's Institute of Technology Ladkrabang, Bangkok 10520, Thailand;* orcid.org/0000-0002-6213-5539; Email: tosapol.ma@kmitl.ac.th

Authors

Tanagorn Sangtawesin − *Thailand Institute of Nuclear Technology (Public Organization), Nakhon Nayok 26120, Thailand*

Phieraya Pulphol − *Advanced Materials Research Unit, School of Science, King Mongkut's Institute of Technology Ladkrabang, Bangkok 10520, Thailand; Department of Materials Science, Faculty of Science, Srinakharinwirot University, Bangkok 10110, Thailand*

Orawan Khamman − *Department of Physics and Materials Science, Faculty of Science, Chiang Mai University, Chiang Mai 50200, Thailand; Center of Excellence in Materials Science and Technology, Materials Science Research Center, Faculty of Science, Chiang Mai University, Chiang Mai 50200, Thailand*

Pakpoom Reunchan − *Department of Physics, Faculty of Science, Kasetsart University, Bangkok 10900, Thailand*

Kazuma Gotoh − *Center for Nano Materials and Technology (CNMT), Japan Advanced Institute of Science and Technology (JAIST), Nomi, Ishikawa 923-1292, Japan*

Naratip Vittayakorn − *Advanced Materials Research Unit, School of Science and Department of Chemistry, School of Science, King Mongkut's Institute of Technology Ladkrabang, Bangkok 10520, Thailand;* orcid.org/0000-0001-9245-0639

Complete contact information is available at: https://pubs.acs.org/10.1021/acs.inorgchem.4c02768

Notes

The authors declare no competing financial interest.

ACKNOWLEDGMENTS

This work is supported by King Mongkut's Institute of Technology Ladkrabang (2567-02-09-001) and "TINT to University" program. Experimental assistance by Kanokwan Chaithaweep is acknowledged. We also acknowledge the facilities and technical assistance from the Nanotechnology and Materials Analytical Instrument Service Unit (NMIS) of the College of Materials Innovation and Technology, KMITL.

REFERENCES

(1) Andersson, S.; Wadsley, A. D. The crystal structure of $Na_2Ti_3O_7$. *Acta Crystallogr.* **1961**, *14*, 1245−1249.

(2) Izawa, H.; Kikkawa, S.; Koizumi, M. Ion exchange and dehydration of layered titanates, $Na_2Ti_3O_7$ and $K_2Ti_4O_9$. *J. Phys. Chem. A* **1982**, *86*, 5023−5026.

(3) Maurya, D.; Kumar, J.; Shripal. Dielectric-spectroscopic and a.c. conductivity studies on layered $Na_{2-X}K_XTi_3O_7$ (X = 0.2, 0.3, 0.4) ceramics. *J. Phys. Chem. Solids* **2005**, *66*, 1614−1620.

(4) Zhang, Y.; Wu, J.; Zhang, Y.; Guo, W.; Ruan, S. Characterization and humidity sensing properties of the sensor based on $Na_2Ti_3O_7$ nanotubes. *J. Nanosci. Nanotechnol.* **2014**, *14*, 4303−4307.

(5) Dynarowska, M.; Kotwiński, J.; Leszczynska, M.; Marzantowicz, M.; Krok, F. Ionic conductivity and structural properties of $Na_2Ti_3O_7$ anode material. *Solid State Ionics* **2017**, *301*, 35−42.

(6) Zarrabeitia, M.; Castillo-Martíneza, E.; Amo, J. M. L. D.; Eguía-Barrio, A.; Muñoz-Márqueza, M. Á.; Rojo, T.; Casas-Cabanas, M. Identification of the critical synthesis parameters for enhanced cycling stability of Na-ion anode material $Na_2Ti_3O_7$. *Acta Mater.* **2016**, *104*, 125−130.

(7) Zarrabeitia, M.; Castillo-Martínez, E.; Del Amoa, J. M. L.; Eguía-Barrio, A.; Muñoz-Márquez, M. A.; Rojo, T.; Casas-Cabanas, M. Towards environmentally friendly Na-ion batteries: Moisture and water stability of $Na_2Ti_3O_7$. *J. Power Sources* **2016**, *324*, 378−387.

(8) Costa, S. I. R.; Choi, Y.-S.; Fielding, A. J.; Naylor, A. J.; Griffin, J. M.; Sofer, Z.; Scanlon, D. O.; Tapia-Ruiz, N. Surface engineering strategy using urea to improve the rate performance of $Na_2Ti_3O_7$ in Na-ion batteries. *Chem. - Eur. J.* **2021**, *27*, 3875−3886.

(9) Tsiamtsouri, M. A.; Allan, P. K.; Pell, A. J.; Stratford, J. M.; Kim, G.; Kerber, R. N.; Magusin, P. C. M. M.; Jefferson, D. A.; Grey, C. P. Exfoliation of layered Na-ion anode material $Na_2Ti_3O_7$ for enhanced capacity and cyclability. *Chem. Mater.* **2018**, *30*, 1505−1516.

(10) Gao, L.; Chen, S.; Zhang, L.; Yang, X. High performance sodium ion hybrid supercapacitors based on $Na_2Ti_3O_7$ nanosheet arrays. *J. Alloys Compd.* **2018**, *766*, 284−290.

(11) Leyet, Y. J.; Guerrero, F.; Anglada-Rivera, J.; de Souza, R. F. B.; Brito, W. R.; Aguilera, L.; Pocrifka, L. A.; Peña-Garcia, R.; Padrón-Hernández, E.; de la Cruz Pérez, J. Synthesis of $Na_2Ti_3O_7$ nanoparticles by sonochemical method for solid state electrolyte applications. *J. Solid State Electrochem.* **2018**, *22*, 1315−1319.

(12) Sriphan, S.; Pulphol, P.; Charoonsuk, T.; Maluangnont, T.; Vittayakorn, N. Effect of adsorbed water and temperature on the universal power law behavior of lepidocrocite-type alkali titanate ceramics. *J. Phys. Chem. C* **2021**, *125*, 12910−12920.

(13) Charoonsuk, T.; Sriphan, S.; Pulphol, P.; Vittayakorn, W.; Vittayakorn, N.; Maluangnont, T. AC conductivity and dielectric properties of lepidocrocite-type alkali titanate tunable by interlayer cation and intralayer metal. *Inorg. Chem.* **2020**, *59*, 15813−15823.

(14) Maluangnont, T.; Pulphol, P.; Pongampai, S.; Kobkeatthawin, T.; Smith, S. M.; Vittayakorn, N. TiO_2/graphitic carbon nitride nanosheet composite with enhanced sensitivity to atmospheric water. *RSC Adv.* **2023**, *13*, 6143−6152.

(15) Thorne, A.; Kruth, A.; Tunstall, D.; Irvine, J. T. S.; Zhou, W. Formation, structure, and stability of titanate nanotubes and their proton conductivity. *J. Phys. Chem. B* **2005**, *109*, 5439−5444.

(16) da Silva, J. P.; Biondo, M. M.; Nobre, F. X.; Anglada-Rivera, J.; Almeida, A.; Agostinho-Moreira, J.; Sanches, E. A.; da, S.; Paula, M. M.; Aguilera, L.; Leyet, Y. Structure and electrical properties of the composite $Na_2Ti_3O_7$/ $Na_2Ti_6O_{13}$/POMA: A study of the effect of adding POMA. *J. Alloys Compd.* **2021**, *867*, No. 159025.

(17) Meng, Y.; Gao, J.; Zhao, Z.; Amoroso, J.; Tong, J.; Brinkman, K. S. Review: recent progress in low-temperature proton-conducting ceramics. *J. Mater. Sci.* **2019**, *54*, 9291−9312.

(18) Maluangnont, T.; Wuttitham, B.; Hongklai, P.; Khunmee, P.; Tippayasukho, S.; Chanlek, N.; Sooknoi, T. An unusually acidic and thermally stable cesium titanate $Cs_xTi_{2-y}M_yO_4$ (x = 0.67 or 0.70; M = vacancy or Zn). *Inorg. Chem.* **2019**, *58*, 6885−6892.

(19) Xu, K.; Qi, C.; Wang, B. Recent progress in research of solid tritium breeder materials Li_2TiO_3: a review. *Coatings* **2022**, *12*, No. 1053.

(20) Dohshi, S.; Anpo, M.; Okuda, S.; Kojima, T. Effect of γ-ray irradiation on the wettability of TiO_2 single crystals. *Top. Catal.* **2005**, *35*, 327−330.

(21) Amin, R. M.; Taha, M.; Moaty, S. A. A.; El-Ela, F. I. A.; Nassar, H. F.; GadelHak, Y.; Mahmoud, R. K. Gamma radiation as a green method to enhance the dielectric behaviour, magnetization, antibacterial activity and dye removal capacity of Co−Fe LDH nanosheets. *RSC Adv.* **2019**, *9*, 32544−32561.

(22) Kaur, S.; Singh, S.; Singh, L.; Lochab, S. P. Effect of gamma irradiation on opto-structural, dielectric, and thermoluminescence properties of natural phlogopite mica. *J. Appl. Phys.* **2013**, *114*, No. 093503.

(23) Nguyen, A. T.; Lee, Y.; Nguyen, P. Q. H.; Dera, P.; Yoon, S.-H.; Lee, W. Enhancing the electrical properties of graphite nanoflake through gamma-ray irradiation. *Sci. Rep.* **2022**, *12*, No. 14824.

(24) Mustafaeva, S. N.; Asadov, M. M.; Ismaïlov, A. A. Effect of gamma irradiation on the dielectric properties and electrical conductivity of the $TlInS_2$ single crystal. *Phys. Solid State* **2009**, *51*, 2269−2273.

(25) Maluangnont, T.; Chaithaweep, K.; Sangtawesin, T.; Khamman, O.; Vittayakorn, N. Fluorine-rich, hydrophobic graphite fluoride with improved charge transport/storage properties produced by gamma irradiation. *J. Phys. Chem. C* **2024**, *128*, 9758−9765.

(26) Maluangnont, T.; Kwamman, T.; Pulphol, P.; Pongampai, S.; Charoonsuk, T.; Pakawanit, P.; Seriwattanachai, C.; Kanjanaboos, P.; Vittayakorn, N. Structural, optical, and electrical properties of cellulose/titanate nanosheets composite with enhanced protection against gamma irradiation. *Ceram. Int.* **2023**, *49*, 31862−31870.

(27) Maluangnont, T.; Chanlek, N.; Suksawad, T.; Tonket, N.; Saikhamdee, P.; Sukkha, U.; Vittayakorn, N. Beyond soft chemistry - bulk and surface modifications of polycrystalline lepidocrocite titanate induced by post-synthesis thermal treatment. *Dalton Trans.* **2017**, *46*, 14277−14285.

(28) Maluangnont, T.; Pulphol, P.; Vittayakorn, W. Interlayer alkali ion governs robustness, reactivity, and dielectric properties of sintered lepidocrocite titanate. *J. Solid State Chem.* **2022**, *305*, No. 122713.

(29) Gorshkov, N. V.; Goffman, V. G.; Vikulova, M. A.; Kovaleva, D. S.; Tretyachenko, E. V.; Gorokhovsky, A. V. Temperature-dependence of electrical properties for the ceramic composites based on potassium polytitanates of different chemical composition. *J. Electroceram.* **2018**, *40*, 306−315.

(30) Maluangnont, T.; Chanlek, N.; Khamman, O.; Vittayakorn, W.; Sooknoi, T. Structural and compositional characteristics of ball-milled lepidocrocite alkali titanate and the correlation to its surface acidic−basic properties. *Inorg. Chem.* **2021**, *60*, 16326−16336.

(31) Maluangnont, T.; Vittayakorn, W. Modifying layered structure of alkali titanates via vibratory ball milling technique. *Integr. Ferroelectr.* **2022**, *223*, 206−213.

(32) Ozawa, T. C.; Sasaki, T. Partial alkali-metal ion extraction from $K_{0.8}(Li_{0.27}Ti_{1.73})O_4$ using PTFE as an extraction agent. *Dalton Trans.* **2014**, *43*, 14902−14908.

(33) Choi, Y.-S.; Costa, S. I. R.; Tapia-Ruiz, N.; Scanlon, D. O. Intrinsic defects and their role in the phase transition of Na-ion anode $Na_2Ti_3O_7$. *ACS Appl. Energy Mater.* **2023**, *6*, 484−495.

(34) Abass, S. A. H.; Seriani, N. Structural and electronic properties of $Na_2Ti_3O_7$ and $H_2Ti_3O_7$. *Phys. Status Solidi B* **2018**, *255*, No. 1700612.

(35) Maluangnont, T.; Vittayakorn, N. Giant dielectric constants in $K_{0.8}M_{0.4}Ti_{1.6}O_4$ (M = Ni, Zn) lepidocrocite-type titanate ceramics. *Integr. Ferroelectr.* **2019**, *195*, 100−108.

(36) Beck, H. P. A DFT study on the correlation between topology and Bader charges: Part III, the development of charge, ″size″ and coordination in alkali and alkaline earth titanates(IV). *Solid State Sci.* **2015**, *48*, 61−71.

(37) Maluangnont, T.; Pulphol, P.; Chaithaweep, K.; Dabsamut, K.; Kobkeatthawin, T.; Smith, S. M.; Boonchun, A.; Vittayakorn, N.

https://doi.org/10.1021/acs.inorgchem.4c02768
Inorg. Chem. XXXX, XXX, XXX−XXX

Alternating current properties of bulk-and nanosheet-graphitic carbon nitride compacts at elevated temperatures. *RSC Adv.* **2023**, *13*, 25276−25283.
(38) Perdew, J. P.; Burke, K.; Ernzerhof, M. Generalized gradient approximation made simple. *Phys. Rev. Lett.* **1996**, *77*, 3865−3868.
(39) Kresse, G.; Furthmüller, J. Efficient iterative schemes for ab initio total-energy calculations using a plane-wave basis set. *Phys. Rev. B* **1996**, *54*, 11169−11186.
(40) Kresse, G.; Furthmüller, J. Efficiency of ab-initio total energy calculations for metals and semiconductors using a plane-wave basis set. *Comput. Mater. Sci.* **1996**, *6*, 15−50.
(41) Petříček, V.; Dusek, M.; Palatinus, L. Crystallographic computing system JANA2006: general features. *Z. Kristallogr.* **2014**, *229*, 345−352.
(42) Belkhiri, S.; Guerza, M.; Chouikh, S.; Boucheffa, Y.; Mekhalif, Z.; Delhalle, J.; Colella, C. Textural and structural effects of heat treatment and γ-irradiation on Cs-exchanged NaX zeolite, bentonite and their mixtures. *Microporous Mesoporous Mater.* **2012**, *161*, 115−122.
(43) Silva, F. L. R. e.; Filho, A. A. A.; da Silva, M. B.; Balzuweit, K.; Bantignies, J.-L.; Caetano, E. W. S.; Moreira, R. L.; Freire, V. N.; Righi, A. Polarized Raman, FTIR and DFT study of $Na_2Ti_3O_7$ microcrystals. *J. Raman Spectrosc.* **2018**, *49*, 538−548.
(44) Łuczyńska-Szymczak, K.; Starosta, W.; Drużbicki, K. Solid-state DFT-assisted Raman study of titanate nanostructures. *Spectrochim. Acta, Part A* **2013**, *116*, 646−650.
(45) Shirpour, M.; Cabana, J.; Doeff, M. New materials based on a layered sodium titanate for dual electrochemical Na and Li intercalation system. *Energy Environ. Sci.* **2013**, *6*, 2538−2547.
(46) Maluangnont, T.; Arsa, P.; Limsakul, K.; Juntarachairot, S.; Sangsan, S.; Gotoh, K.; Sooknoi, T. Surface and interlayer base-characters in lepidocrocite titanate: the adsorption and intercalation of fatty acid. *J. Solid State Chem.* **2016**, *238*, 175−181.
(47) Promchana, P.; Boonchun, A.; T-Thienprasert, J.; Sooknoi, T.; Maluangnont, T. Direct conversion of carboxylic acid to olefins over Pt-loaded, oxygen-deficient alkali hexatitanate catalysts with ketonization-hydrogenation-dehydration activity. *Catal. Today* **2021**, *375*, 418−428.
(48) Akimoto, J.; Chiba, K.; Kijima, N.; Hayakawa, H.; Hayashi, S.; Gotoh, Y.; Idemoto, Y. Soft-chemical synthesis and electrochemical property of $H_2Ti_{12}O_{25}$ as a negative electrode material for rechargeable lithium-ion batteries. *J. Electrochem. Soc.* **2011**, *158*, A546−A549.
(49) Schulz, H. From the Kissinger equation to model-free kinetics: reaction kinetics of thermally initiated solid-state reactions. *ChemTexts* **2018**, *4*, No. 9.
(50) Sarı Yılmaz, M.; Kasap, S.; Pişkin, S. Preparation, characterization and thermal dehydration kinetics of titanate nanotubes. *J. Therm. Anal. Calorim.* **2013**, *112*, 1325−1333.
(51) Tong, L.; Sun, J.; Wang, S.; Guo, Y.; Li, Q.; Wang, H.; Wang, C. Normal and abnormal dielectric relaxation behavior in $KTaO_3$ ceramics. *RSC Adv.* **2017**, *7*, 50680−50687.
(52) Kubliha, M.; Trnovcová, V.; Ondruška, J.; Štubňa, I.; Bošák, O.; Kaljuvee, T. Comparison of dehydration in kaolin and Illite using DC conductivity measurements. *Appl. Clay Sci.* **2017**, *149*, 8−12.
(53) Maluangnont, T.; Pulphol, P.; Klangvijit, K.; Bowornthommatadsana, K.; Chanlek, N.; Ogawa, M.; Wongwiriyapan, W. Electrochemical and electrical characteristics of ball milled $Cs_2Ti_6O_{13}$ modified by the surface-to-bulk migration of hydroxyl groups. *Dalton Trans.* **2023**, *52*, 11815−11825.
(54) Maluangnont, T.; Sriphan, S.; Charoonsuk, T.; Vittayakorn, N. Dielectric spectroscopy and electric modulus analyses of $Ti_{0.8}O_2$ nanosheets−Ag nanoparticles−cellulose filter paper composites. *Integr. Ferroelectr.* **2022**, *224*, 214−224.
(55) Baliteau, S.; Sauvet, A.-L.; Lopez, C.; Fabry, P. Controlled synthesis and characterization of sodium titanate composites $Na_2Ti_3O_7/Na_2Ti_6O_{13}$. *Solid State ionics* **2007**, *178*, 1517−1522.
(56) Jonscher, A. K. Dielectric relaxation in solids. *J. Phys. D: Appl. Phys.* **1999**, *32*, R57−R70.
(57) Jonscher, A. K. The 'universal' dielectric response. *Nature* **1977**, *267*, 673−679.
(58) Jonscher, A. K. Low-frequency dispersion in volume and interfacial situations. *J. Mater. Sci.* **1991**, *26*, 1618−1626.

https://doi.org/10.1021/acs.inorgchem.4c02768
Inorg. Chem. XXXX, XXX, XXX−XXX